Different responses of phytoplankton to Fe manipulation in Fe-limited waters with contrasting surface mixed layer depths in the western subarctic Pacific

Kazuhiro Yoshida[1†], Jun Nishioka[1,3], Ichiro Yasuda[4], Koji Suzuki[1,2]

[1]Graduate School of Environmental Science, Hokkaido University, N10W5, Kita-Ku, Sapporo, Hokkaido 060-0810 Japan

[2]Faculty of Environmental Earth Science, Hokkaido University, N10W5, Kita-Ku, Sapporo, Hokkaido 060-0810 Japan

[3]Pan-Okhotsk Research Center, Institute of Low Temperature Science, Hokkaido University, N19W8, Kita-Ku, Sapporo, Hokkaido 060-0819 Japan

[4]Atmosphere and Ocean Institute, The University of Tokyo, 5-1-5, Kashiwanoha, Kashiwa, Chiba, 277-8564 Japan

[†]Present address: Faculty of Agriculture, Saga University, 1 Honjo-Machi, Saga, Saga 840-8502 Japan

Corresponding authors: Kazuhiro Yoshida: sv8269@cc.saga-u.ac.jp; Koji Suzuki: kojis@ees.hokudai.ac.jp

ORCID: Kazuhiro Yoshida 0000-0001-5768-8561

Jun Nishioka 0000-0003-1723-9344

Ichiro Yasuda 0000-0002-4742-6880

Koji Suzuki 0000-0001-5354-1044

Keywords: Fe-light co-limitation; vertical mixing; on-deck Fe-manipulation experiment; phytoplankton photophysiology; scanning electron microscopy

Abstract

In the western subarctic Pacific (WSP), iron (Fe) can enhance the biological carbon pump by stimulating phytoplankton photosynthesis. However, little is known about how Fe and light availability controls the phytoplankton photophysiology in the WSP near the Kuril Islands, where water mixing is sometimes enhanced, even in summer. Here, we conducted on-deck Fe-manipulated incubation experiments at two stations where surface mixed layer depths were distinct but showed similar initial macronutrient and dissolved Fe concentrations and phytoplankton community composition even experienced light availability for phytoplankton in the water column could be different. An Fe addition to water samples from the deeper surface mixed layer enhanced the phytoplankton biomass and the photosynthetic competence in photosystem II (F_v/F_m), suggesting an Fe-light co-limitation, which was supported by the results from high functional absorption cross-section of photosystem II (σ_{PSII}) and low light saturation index (E_k). At the shallower mixed layer station, Fe amendment did not stimulate phytoplankton biomass and photosynthesis, indicating that Fe was sufficient for the phytoplankton. Although the centric diatom *Chaetoceros* species were predominant at both stations throughout incubation, the pennate diatoms *Pseudo-nitzschia* spp. and *Cylindrotheca closterium* significantly increased at the deeper- and shallower-mixed layer stations, respectively, after Fe enrichment. The elongation of the pennate diatom *Neodenticula seminae* chains was observed under low Fe availability caused by a chelator. This could be related to the fact that *N. seminae* is abundant in sediment trap samples from the WSP under Fe-limited conditions and contributed to the high biological pump efficiency.

1. Introduction

Iron (Fe) plays a central role in algal photosynthetic processes such as pigment synthesis, electron transfer via iron-related proteins, nitrate reduction, and detoxification of reactive oxygen (Sunda and Huntsman, 1995; Twining and Baines, 2013; Behrenfeld and Milligan, 2013). *In situ* mesoscale Fe fertilization experiments have revealed that Fe availability controls phytoplankton biomass and primary productivity in High Nutrient, Low Chlorophyll (HNLC) waters (e.g., Boyd et al., 2007). The western subarctic Pacific (WSP) is known as an HNLC region with unique biogeochemical features from spring to summer (Harrison et al., 1999; Tsuda et al., 2003; Suzuki et al., 2009; Hattori-Saito et al., 2010; Fujiki et al., 2014; Nishioka et al., 2020). An *in situ* Fe fertilization in the Western Subarctic Gyre of the WSP during summer stimulated the growth of large diatoms (> 10 μm) and their export (Tsuda et al., 2003), which suggests that the WSP has significant potential to

sequestrate carbon after natural Fe fertilization compared with other major HNLC waters (de Baar et al., 2005). Indeed, during springtime, it has been reported that the WSP has high transport efficiencies of particulate organic carbon (Honda, 2003; Kawakami et al., 2004; 2015) and consequently has the most prominent biological drawdown of CO_2 among the world's oceans (Takahashi et al., 2002).

Nishioka et al. (2007, 2013, 2014, 2020) and Nishioka and Obata (2017) demonstrated that the Dense Shelf Water (DSW) in the Sea of Okhotsk transports sedimentary Fe from the continental shelf to the North Pacific Intermediate Water (NPIW) via the straits of the Kuril Islands where intense vertical mixing occurs. This upward Fe supply fertilizes coastal waters along the Kuril Islands in the WSP (Nishioka et al., 2020). Yoshida et al. (2020) also confirmed that, by conducting photophysiological measurements, coastal communities on the shelf around the Kuril Island Chain were in Fe-repleted conditions for their growth, whereas offshore communities were starved for Fe availability. Yoshida et al. (2020) also reported that, even though the macronutrient and Fe concentrations were similar among the HNLC waters, the offshore phytoplankton showed diverse primary productivity, ranging from 19.0−161.4 mg C m^{-3} d^{-1}. The various photosynthetic status implies that other environmental parameters regulate the photosynthesis activity of the Fe-limited phytoplankton communities. In general, primary productivity (photosynthetic rate) can be defined by the combination of biomass, light availability, and photosynthetic physiology (Bannister, 1974). Yoshida et al. (2020) suggested that light availability, in terms of the ratios of euphotic zone and mixed layer depths, was a crucial controlling factor for primary productivity in the WSP during summer.

Low Fe availability reduces the activity and amount of photosystems I and II (Greene et al., 1992; Geider and LaRoche, 1994). The resultant reduced abundance of Fe-related photosynthetic components consequently hinders electron transport and algal pigment synthesis in the photosystems, as mentioned above. Sunda and Huntsman (1997) reported, by conducting culture-based incubation experiments, that co-limitation of Fe and light further limited the photosynthetic processes of phytoplankton; algal cells at lower light conditions require more Fe to maintain their photosynthesis. This antagonistic Fe-light co-limitation has also been reported on natural phytoplankton communities in subarctic waters and Antarctic diatoms (Maldonado et al., 1999; Strzepek et al. 2012; 2019; Alderkamp et al., 2019). Also, in the WSP, the antagonistic Fe-light co-limitation has been suggested in well-mixed water columns near the straits around the Kuril Islands (Yoshimura et al., 2010; Sugie et al., 2013; Suzuki et al., 2014). For the water mixing processes, (1) strong vertical mixing in straits (Ono et al., 2010; Yagi and Yasuda, 2012), and (2) mesoscale eddies along the Kuril-Kamchatka Trench (Yasuda, 2000; Kaneko et al., 2015) have been documented. It is, thus, needed to understand how Fe and light availability

interact to disentangle the diverse photosynthetic physiology of phytoplankton in Fe-limited waters in the WSP.

We conducted on-deck Fe-manipulated incubation experiments combined with multiple photosynthetic measurements to discuss how Fe and light availabilities affect the photosynthetic physiology of phytoplankton in the WSP near the Kuril Islands. Then, we collected seawater from two stations with similar macronutrient concentrations but contrasting surface mixed layer depths (MLD; 28.5 m and 12.8 m). Effects of Fe amendment plus light acclimation states were assessed with carbon-based photosynthesis−irradiance relationships and variable chlorophyll *a* fluorescence, which can provide powerful insights into the physiological acclimation of phytoplankton (Sakshaug et al., 1997; MacIntyre et al., 2002; Suggett et al., 2009; Bouman et al., 2018). The community composition of phytoplankton was also monitored with scanning electron microscopy and flow cytometry during the Fe-manipulated incubation experiments to investigate which species/groups respond to enhanced Fe availability.

2. Materials and methods

2.1. Experimental setup

During the R/V *Professor Multanovskiy* cruise (Mu14 expedition) in the summer of 2014, using trace-metal-clean techniques, surface seawater was collected for two Fe-manipulated on-deck incubation experiments in the western subarctic Pacific off the eastern Kamchatka Peninsula (Station C5, 52° 00′ 07 N, 160° 10′ 34 E) and the Kuril Islands (Station A5, 45° 26′ 39 N, 152° 58′ 38 E) on 18 and 28 June 2014, respectively (Fig. 1). Seawater was obtained from 5 m layer and 5% light depths around noon using a CTD (SBE 9 plus, SeaBird Ltd.) and carousel multi-sampler (SBE32, SeaBird Ltd.) system (CTD-CMS) with acid-cleaned Teflon-coated 10 L Niskin-X bottles (Obata et al., 1993; Takeda and Obata, 1995; Nishioka et al., 2001). Mixed layer depths were defined where the potential density anomaly ($\Delta\sigma_\theta$) of the water column was 0.125 kg m^{-3} larger than the sea surface at 10 m (Monterey and Levitus, 1997). The 5% light depths were determined based on the diffusive attenuation coefficients of photosynthesis available radiation (PAR) (K_d(PAR)) calculated from *in situ* vertical PAR profiles using a Compact-Optical Profiling System (Biospherical Instruments Inc.) (Hooker et al., 2013) and the National Aeronautics and Space Administration Processing of Radiometric Observations of Seawater using Information Technologies (PROSIT) software (Hooker et al., 2018) with reference to the incident PAR (E_0(PAR)) above the sea surface. Euphotic zone depths were defined as 1% light depth compared to E_0(PAR) (Kirk, 2010). The surface seawater from 5 m was dispensed into eight trace-metal-cleaned 9 L polycarbonate (PC) bottles without pre-filtration. Two out of the eight bottles were Fe-enriched by adding $FeCl_3$ solution (final

Fe concentration of 10 nM; hereafter, +Fe treatments). For another set of two PC bottles, the Fe chelator deferoxamine B was amended (final concentration of 1 μM, hereafter +DFB treatments) to reduce Fe availability for phytoplankton (e.g., Wells, 1999; Hutchins et al., 1999; Kondo et al., 2013). The other two bottles were used as controls without any addition (hereafter Control), whereas another set of two bottles were time-zero (hereafter Initial). The six bottles, except for Initials, were double-wrapped with transparent plastic bags to prevent contamination and incubated in a temperature-controlled on-deck incubator at *in situ* temperature and natural light environment (100% surface light) for 3–4 days. Unfortunately, one of the +DFB bottles incubated at station A5 was contaminated due to water seeping into the bottle (discussed in section 3.4).

Vertical water-column stability (i.e., stratification) at MLD was estimated from Brunt-Väisälä frequency (N^2), which was calculated on 3-m moving-averaged temperature-salinity profiles (Wahl and Teague, 1983; Schaffer et al., 2012):

$$N^2 = (g / \rho) \cdot (\partial\rho / \partial z) \quad (1)$$

where g is gravitational acceleration, ρ is seawater density at each depth (kg m^{-2}), and z is depth. Besides, upward fluxes, across the mixed layer of nitrate and dissolved iron (DFe) were quantified as F_{NO3} and F_{DFe} based on the vertical diffusivity according to Osborn (1980) and Kaneko et al. (2013):

$$F_{NO3} = K_\rho \cdot \partial NO_3 / \partial z \quad (2)$$

$$F_{DFe} = K_\rho \cdot \partial DFe / \partial z \quad (3)$$

$$K_\rho = \Gamma \varepsilon / N^2 \quad (4)$$

where K_ρ is vertical diffusivity to estimate upward nutrient flux derived from the micro-temperature observations using MicroRider MR6000 (Rockland Scientific) attached to the CTD-frame. The MR6000 was equipped with FP07 (Fastip Probe #7) fast-response thermistor. Turbulent energy dissipation rate ε and turbulent thermal dissipation rate χ were estimated from temperature gradient spectra following the procedures with the time-constant corrections of double-pole 3 ms (Goto et al. 2016, 2018, 2021; Yasuda et al. 2021), in which the measurements were confirmed to be valid in the ranges of $10^{-11} < \varepsilon < 10^{-8}$ (W kg^{-1}) and $10^{-11} < \chi < 10^{-7}$ (°C^2 s^{-1}). Vertical diffusivity K_ρ is then computed as $K_\rho = 0.2\ \varepsilon\ N^{-2}$ (m^2 s^{-1}) (Osborn, 1980) where 10-dbar mean squared buoyancy frequency N^2 using CTD density data. The shallow part (< 100 m depth) of the ε data at stations C5 and A5 was expected to be underestimated, considering the measurement of the upper limit (ε =

~10^{-8} W kg^{-1}) near the surface. In this study, for the upper 100 m, temperature dissipation χ was alternatively used for the estimate of the vertical diffusivity (Osborn and Cox, 1972):

$$K_T = 0.5\ \chi\ \theta_z^{-2} \quad (5)$$

where θ_z is the vertical gradient of potential temperature θ because χ is less underestimated than using ε (Goto et al., 2018). Differences in average nitrate and DFe concentration from 10–50 m depths were represented as $\partial NO_3/\partial z$ and $\partial DFe/\partial z$, respectively. Also, we used the averaged K_T value from 10 m to 50 m depths to estimate F_{NO3} and F_{DFe}. To discuss the potential Fe limitation for phytoplankton photosynthesis, the upward flux ratio, F_{DFe} / $F_{NO3,}$ was calculated:

$$F_{DFe} / F_{NO3} = (\partial DFe/\partial z)/ (\partial NO_3/\partial z) \quad (6)$$

2.2. Total dissolvable Fe analysis

Before and after the incubation experiments, total dissolvable Fe (TFe) samples in each 9 L PC bottle were collected into an acid-cleaned 125 mL LDPE bottle. The samples were acidified with 20% ultrapure HCl (Tamapure AA-10, Tamapure Co., Ltd.) to solubilize all labile Fe in seawater (Obata et al., 1997). Samples were buffered with 10 M formic acid - 2.4 M ammonium formate buffer to adjust pH to 3.2 just before measurements on land. Concentrations of TFe were determined with an automatic Fe (III) flow injection analytical system (Kimoto Electric, Ltd.) with pre-concentration by a chelating resin following the chemiluminescence method (Obata et al., 1993; 1997). The concentration of TFe in the DFB treatments was not able to be quantified due to the strong ligand complexation. All ambient DFe (< 0.2 μm) data used in the discussion section of this study were cited from Nishioka et al. (2020) and Nishioka et al. (2021).

2.3. Phytoplankton pigment analysis

Phytoplankton biomass in each treatment was estimated from the sum of chl *a* and its derivatives (i.e., chl *a*-allomer, chl *a*-epimer, and chlorophyllide *a*) determined with High-Performance Liquid Chromatography (HPLC). Triplicated water samples taken from each 9 L PC bottle, before and after the incubation experiments, were filtered onto 25 mm GF/F filters (Whatman) under gentle vacuum (<0.013 Mpa). The filters were flash-frozen in liquid nitrogen and stored in a deep freezer (−80 °C) until analysis on land. The frozen filter was blotted with a qualitative filter paper, snipped, and sonicated in 3 mL of *N*,*N*-dimethylformamide (DMF)

containing a known amount of canthaxanthin as an internal standard to extract algal pigments (Suzuki et al., 2002). The pigment extracts were passed through a 0.45 μm PTFE filter to remove fine particles. The pigment extracts of 250 μL were mixed with 28 mM tetrabutylammonium acetate aqueous solution of the same quantity, and the mixture was injected into an HPLC (CLASS-VP System, Shimadzu) with an Agilent Eclipse XDB C8 column (3.5 μm particle size, 4.6×150 mm) following Endo et al. (2013).

2.4. Photosynthesis−irradiance (*P-E*) relationship measurement

The seawater from each 9 L PC bottle was dispensed into twelve 275-mL polystyrene bottles. A ^{13}C-labelled sodium bicarbonate ($NaH^{13}CO_3$, 99 atom% ^{13}C, Cambridge Isotope Laboratories, Inc.) solution was added to ten bottles (ca. 10% of total dissolved inorganic carbon). The remaining two bottles were initial samples used as a ^{13}C background for each bottle. A series of ^{13}C-labeled seawater in 10 bottles was incubated for 2 h in a temperature-controlled incubator at 10 different light intensities from 1.44 to 3,000 μmol photons m^{-2} s^{-1} and at the *in situ* temperatures (Table 1). After 2 h incubation, the samples were filtered onto pre-combusted 25 mm GF/F filters (Whatman) with a gentle vacuum in the dark (<0.013 MPa) and stored in a deep freezer (−80 °C) until further analysis on land. The amount of ^{13}C on the filters was measured with an online element analyzer (FlashEA1112, Thermo Finnigan)/Isotope ratio mass spectrometer (EA/IRMS) (Delta-V, Thermo Finnigan). The photosynthesis rates of phytoplankton were calculated following Hama et al. (1983). The resultant photosynthesis rate was normalized with chl *a* concentration to obtain chl *a*-specific photosynthesis rate (P^B). A set of P^B values and the corresponding irradiance in the bottles were fitted with the photosynthesis−irradiance (*P-E*) relationship model of Platt et al. (1980) (Fig. 3).

2.5. Variable chlorophyll *a* fluorescence

Photosynthetic physiological responses, including light acclimation, to Fe manipulation were also assessed with the maximum photochemical quantum yield and functional absorption cross-section of photosystem II (PSII) for phytoplankton using variable chl *a* fluorometry. Variable chl *a* fluorescence *in situ* was measured with a Fluorescence Induction and Relaxation (FIRe) fluorometer (Satlantic Inc.). Natural seawater samples at 5 m and 5% light depth (C5: 26.0 m; A5: 23.6 m) were collected into a 30 mL shading polyethylene bottle, whereas seawater from the Fe-manipulated incubation bottles was dispensed into another shading bottle. The samples were incubated in darkness at *in situ* temperature for 30 minutes for dark acclimation. A single turnover excitation protocol was applied to the dark-acclimated cells with 80 μs flash at 450 nm from a light-emitting

diode (LED) equipped with the FIRe fluorometer. Chl *a* fluorescence induction curves were iterated 10 times after 1000 ms intervals between each flash. The obtained induction curves were averaged and fitted to the model proposed by Kolber et al. (1998) using the MATLAB-based program fireworx developed by Audrey Barnett (Dalhousie University). The maximum quantum yield of PSII photochemistry (F_v/F_m) and functional absorption cross-section of PSII (σ_{PSII}; $Å^2$ $quanta^{-1}$) were obtained from the resultant fitted curves. The difference in σ_{PSII} values between samples from the surface and the depth of the 5% light level was defined as $\Delta\sigma_{PSII}$.

2.6. Microscopy

Armored phytoplankton cells were enumerated with scanning electron microscopy (SEM) to examine community shifts after Fe manipulation. Five hundred milliliters of seawater in each bottle were fixed with a neutral formaldehyde solution buffered with sodium acetate (final concentration 2%). A subsample of the fixed sample was filtered onto a 25 mm, 0.4 μm Nuclepore membrane filter set on a glass funnel under gentle vacuum (< 0.013 Mpa). After rinsing the filter with distilled water for desalination, the filter was coated with Au-Pb alloy using an MSP-1S magnetron spatter device (Vacuum Device Inc.). Armored protistan cells were counted with a scanning electron microscope (VE-8800, Keyence Co., Ltd.) with a magnification of >1000×, according to Nosaka et al. (2014, 2017). For each sample, >3000 cells were enumerated. Species identification was based on Tomas (1997), Round et al. (2007), Konno et al. (2007), and Medvedeva and Nikulina et al. (2014). The number of plastids in *Chaetoceros* cells was enumerated by bright-field microscopy (Keyence BZ-9000).

2.7 Flow cytometry

Ultraphytoplanktonic (< 10 μm in size) cryptophytes and *Synechococcus* were enumerated with flow cytometry (FCM) to complement SEM, which cannot identify small unarmoured phytoplankton. Two milliliters of seawater samples from each bottle were fixed with 40 μL of 10 % paraformaldehyde (PFA) in a cryovial (final concentration 0.2 %). The seawater samples in the vials were flash-frozen in liquid nitrogen and stored in a deep freezer (–80 ºC) until analysis on land. Enumeration of ultraphytoplankton cells was performed with an EPICS flow cytometer (XL ADC system, Beckman Coulter) equipped with 15 mW air-cooled laser exciting at 488 nm. The FCM samples were melted gradually in distilled water and prefiltered through a 35 μm nylon-mesh-capped Falcon cell strainer (Becton-Dickinson) to remove larger cells before loading to the FCM. Each sample was analyzed with the EXPO32 software (Beckman Coulter) as described in Suzuki et al. (2005).

3. Results

3.1. Hydrography

Sea surface temperature and salinity at 5 m (hereafter, SST and SSS, respectively) were similar and generally low at both stations (C5: 6.05 ºC, 32.77; A5: 6.80 ºC, 32.81, Fig. 1 and Table 1). Macronutrient concentrations at 5 m of the two stations were also similar to each other and relatively high. Fe concentration was low at the two stations (C5: 0.05 nM DFe; A5: 0.06 nM DFe, Nishioka et al., 2020, 2021) (Table 1). Both stations showed rather similar euphotic layer depths (Z_{eu}; C5: 40.3 m; A5: 36.2 m). In contrast, the surface mixed layer depths (MLDs) were contrastive; station C5 showed a deep MLD (28.5 m), whereas station A5 showed a shallow MLD (12.8 m) (Table 1). Note that MLDs at stations C5 and A5 were the deepest and the second shallowest throughout the Mu14 expedition (Yoshida et al., 2020). Although the vertical water-column stability (N^2) within the MLDs was comparable between the two stations (C5: 9.82×10^{-2} s^{-1}; A5: 9.82×10^{-2} s^{-1}; Table 1), the upward fluxes of NO_3 and DFe at station C5 were 10-times higher than those at station A5 (C5: F_{NO3} = 2.82 × 10^3 mmol m^{-2} day^{-1}, F_{DFe} = 32.7 μmol m^{-2} day^{-1}; A5: F_{NO3} = 297 mmol m^{-2} day^{-1}, F_{DFe} = 3.11 μmol m^{-2} day^{-1}, Table 1), where F_{NO3} and F_{DFe} were comparable with those reported in Nishioka et al. (2020), although their flux data were calculated based on different depths from the present study. The resultant upward flux ratios of DFe to NO_3 (F_{DFe} /F_{NO3}) were similar between the two stations (C5: 0.0112 mM μM^{-1}; A5: 0.0105 mM μM^{-1}, Table 1).

Concentrations of TFe after the incubation experiments showed similar patterns at both stations (Fig. 2). The highest TFe was derived from the Fe-added bottles, followed by the initial (i.e., time-zero) and control treatments (Fig. 2).

3.2. Responses of photosynthetic parameters to Fe and DFB addition

A large increase in chl *a* concentration after Fe addition was observed at station C5 compared to the control treatment (2.2-times higher, Fig. 4). Of all the bottles at station C5, the +DFB bottles had the lowest chl *a* value, although little difference was found as compared to the Control bottles (Fig. 4). At station A5, on the other hand, the concentrations of chl *a* in the Control and +Fe bottles were increased by 30% from the Initial, while the DFB bottle showed the second lowest following the Initial (Fig. 4). At station A5, one out of the +DFB bottles was contaminated with external Fe due to the immersion of waters into bottles, the results from the contaminated bottle were thus excluded from further discussion.

The F_v/F_m values between stations C5 and A5 behaved similarly with the response of chl *a* after the Fe and DFB amendment (Fig. 5A). After Fe addition at station C5, the F_v/F_m values increased by 43.7% compared with the Control treatment (Fig. 5A), while DFB amendment showed the lowest F_v/F_m value (0.175), which was far lower than the Control and +Fe treatments. At station A5, a small difference (10%) in F_v/F_m was observed between the Control and +Fe treatments (Fig. 5A). The F_v/F_m values for +DFB treatments at both stations were almost identical or lower than the initial values. FIRe fluorometry showed that the values of σ_{PSII} decreased after the incubation experiments compared to the Initial at both stations. However, the σ_{PSII} further decreased in the +Fe bottles at station C5, whereas those in the Control and +Fe bottles were comparable at station A5 (Fig. 5B). Also, the σ_{PSII} in the +DFB bottles showed relatively high, which was comparable to the Initial at station C5, while the σ_{PSII} values were almost comparable among the treatments (Fig, 5B). FIRe fluorometry also provided σ_{PSII} values in the Initial at the surface and 5% light depths at both stations. Little variation in σ_{PSII} was found at station C5 between the samples collected from the surface and 5% light depth (5 m: 328±10 $Å^2$ $quanta^{-1}$, 5%: 326±28 $Å^2$ $quanta^{-1}$, i.e., $\Delta\sigma_{PSII}$=2 $Å^2$ $quanta^{-1}$), whereas the $\Delta\sigma_{PSII}$ at station A5 was large (5 m: 332±18 $Å^2$ $quanta^{-1}$, 5%: 403±34 $Å^2$ $quanta^{-1}$, i.e., $\Delta\sigma_{PSII}$=71 $Å^2$ $quanta^{-1}$) (Fig. 7). The 5% light depth (26.0 m) at station C5 was comparable to the MLD, whereas the 5% light depth at station A5 was much deeper than the MLD.

Photosynthetic-irradiance (*P-E*) parameters showed different responses to the Fe and DFB amendment between stations C5 and A5 (Fig. 6). At station C5, *P-E* parameters little changed between the Control and +Fe treatments, whereas the DFB amendment significantly lowered only P^B_{max} (2.38±0.73 mg C mg chl a^{-1} hr^{-1}) compared to the Control (9.09±1.58 mg C mg chl a^{-1} hr^{-1}) and +Fe treatments (10.08±1.75 mg C mg chl a^{-1} hr^{-1}). The Fe amendments to the A5 seawater largely increased the α^B values (Control: 0.045±0.013 (mg C mg chl a^{-1} hr^{-1}) (μmol photons m^{-2} s^{-1})$^{-1}$, +Fe: 0.053±0.003 (mg C mg chl a^{-1} hr^{-1}) (μmol photons m^{-2} s^{-1})$^{-1}$, Fig. 6A); however, the other *P-E* parameters did not respond to the Fe addition (Fig. 6B, C, D). The increment of E_k between Initial and Control was doubled at station C5, while that at station A5 was small (Fig. 6D).

3.3. Community responses to Fe and DFB addition

The abundance of coccolithophores and Parmales decreased during incubation at station C5, while *Chaetoceros* species dominated in the Control and +Fe bottles at the station (Tables 2 and S1). *Pseudo-nitzschia* spp. was the only species showing a remarkable increase after +Fe addition. Interestingly, in the +DFB treatment, *Cheatoceros* species were replaced with large and robust diatoms (e.g., *Corethron pennatum*, *Neodenticula seminae*, and *Thalassionema nitzschioides*) with an increase in *Fragilariopsis* species and armored

ciliates at station C5 as well as resting spores of *Chaetoceros* (Tables 2 and S1). The abundance of *Chaetoceros* species, which were initially dominant, was also the highest in the control bottles, followed by +Fe bottles at station C5. *Pseudo-nitzschia* spp. also increased both in the Control and +Fe bottles, while *Cylindrotheca closterium* greatly increased only in the +Fe treatment.

At station A5, *Chaetoceros* species were predominant both in the Control and +Fe bottles. In contrast, the large and robust species (i.e., *C, pennatum*, *N. seminae*, and *T. nitzschioides*) outcompeted the community in +DFB bottles, replacing the *Chaetoceros* species except for *Ch. concavcornis* and *Ch. convolutus*, which increased in abundance (Tables 2 and S1). Length of chains of *Neodenticula seminae* were often long (>5 up to 23 cells in a chain) in the +DFB bottles at both stations, although solitary cells or short chains of the species were generally observed at the other stations and in the other bottles (Fig. 8, Table 2).

The Fe addition enhanced the abundance of cryptophytes, whereas *Synechococcus* did not respond to Fe manipulations at the two stations (Fig. 9). Cryptophytes considerably grew up in the +Fe treatments compared with the Control and +DFB treatments at station C5 (~2.5-times and ~2-times higher compared with Control and +DFB treatments, respectively). Also, at station A5, the abundance of cryptophytes largely increased in the +Fe treatment compared with the Control treatment (1.90-times higher) (Fig. 9A). The abundance of *Synechococcus*, on the other hand, did not change throughout the incubation both at stations with slight decreases (Fig. 9B).

4. Discussion

The initial community structures at both stations were relatively similar (Tables 2 and S1), although their photosynthetic responses to Fe or DFB additions differed. At station C5, a remarkable increase in chl *a* was observed after the Fe addition as compared with that of the Control treatment (Fig. 4), suggesting that Fe limitation occurred. The large increase in F_v/F_m values after Fe addition supported this notion (Fig. 4A). The Fe addition to the algal assemblages at station A5 did not show little variation in chl *a* (Fig. 4) between the Control and +Fe bottles. The F_v/F_m values also responded less to the Fe amendment at station A5 (Fig. 5A), indicating Fe repletion for the phytoplankton assemblage, in spite of the low dissolved Fe concentration (DFe=0.05 nM; Table 1, Nishioka et al., 2020; 2021). However, the upward fluxes of NO_3 and DFe were much higher at station C5 than those at station A5 (Table 1). The phytoplankton assemblage at station C5 would thus be more accessible to Fe from below the MLD than at station C5 (Table 1). Note that the upward flux ratios (F_{DFe}/F_{NO3}) were relatively low between the two stations (Table 1). Browning et al. (2017) and Shaked et al. (2021)

suggested that Fe could be the primary limiting nutrient even if DFe/NO_3 ratios were low (0.01−0.016), indicating that the phytoplankton assemblages at both stations in this study were potentially Fe-limited compared with nitrate availability even if the deepwater uplifted.

Even potential Fe availability was low at both stations, the ^{13}C-based photosynthetic performance interestingly showed little changes after Fe addition. Interestingly, the ^{13}C-based photosynthetic performance showed little changes, even though the biomass was enhanced after Fe addition at station C5 (Figs. 4 and 6). These physiological responses indicate the phytoplankton assemblages at this station prioritized pigment synthesis over carbon fixation when Fe was supplied. Indeed, the increased Fe availability reduced the light-harvesting antennae size of PSII, σ_{PSII} (Fig. 5B) with the F_v/F_m and chl *a* enhancement (Figs. 4 and 5A), which are similar to PSII reorganization to improve the energy funneling from light-harvesting antennae to the reaction center of PSII (Suggett et al. 20009). D'Haene et al. (2015) and Yoshida et al. (2018) demonstrated that PSII antennae are restructured with a decrease in σ_{PSII} and an increase in F_v/F_m with significant increases in the number of the reaction center of PSII (n_{PSII}). This relative increase in n_{PSII} consequently reduces σ_{PSII}. This is because the +DFB bottles showed relatively high σ_{PSII} values due to unsuccessful antennae reorganization under severe Fe-limitation (Fig. 5B). In another aspect from bio-optics, deeper MLD had smaller E_k and vice versa in the studied area (Yoshida et al. 2020), indicating that phytoplankton in the study area had been well-acclimated to light environments. The phytoplankton assemblages at station C5, where the MLD was 28.5 m, had a low E_k for the Initial (i.e., low light-acclimated), whereas that at station A5, where the MLD was 12.8 m, was higher (i.e., high light-acclimated). The inherent photophysiological status of the phytoplankton assemblages (e.g., pigmentation and cellular Fe requirement) might differ between the two stations. The difference in the degree of light acclimation between the phytoplankton at stations C5 and A5 was supported by the results of $\Delta\sigma_{PSII}$ (Fig. 8). The smaller $\Delta\sigma_{PSII}$ value at station C5 suggested the water column was well mixed, therefore the phytoplankton would experience lower average light intensity in the water column, which supports the low E_k value for the Initial. The large $\Delta\sigma_{PSII}$ value at station A5 suggested the phytoplankton acclimated to the light intensity at each depth, specifically due to the shallow MLD (Figs. 6 and 8). The phytoplankton assemblages at station C5 were thus acclimated to a dimmer environment, indicating that Fe-light co-limitation likely occurred at the station as suggested by Suzuki et al. (2014) in the well-mixed water columns in the WSP near the Kuril Islands., which could exacerbate Fe-light co-limitation for the phytoplankton assemblage. This notion was supported by the doubled increment of E_k between Initial and Control at station C5. The results suggest that the initial phytoplankton cells suffered from light limitation (Fig. 6D). However, the phytoplankton assemblage at

station A5 might employ other strategies, enhancing the carbon fixation activity (i.e., a significant increase in α^B; Fig. 6A). Greene et al. (1992), Geider and LaRoche (1994), and McKay et al. (1997) discussed that phytoplankton could decrease the ratio of more Fe-requiring PSI/cytochrome b_6/f complex to less Fe-requiring PSII. In addition, Strzepek et al. (2012, 2019) demonstrated that phytoplankton increases photosynthetic antenna size (i.e.,σ_{PSII}) rather than the number of antennae under Fe-deficient conditions, which does not associate with little change in chl *a* concentration. This notion was also supported by the comparable σ_{PSII} values among the treatments (Fig. 5B), indicating that phytoplankton did not need to reorganize the PSII antennae even with Fe manipulations. The Fe-replete (or slightly Fe-starved) phytoplankton at station A5 might thus prioritize modifying their photosynthetic architecture without chl *a* increase or changes in σ_{PSII} and n_{PSII} (Figs. 4 and 5B). At both stations, DFB inhibited the growth of phytoplankton compared to the Control due to its strong Fe complexation capability even though the Fe concentration was low (Table 1). However, chl *a* in the DFB treatment at station A5 increased than the Initial condition (Fig. 4) despite the Fe chelation. This increase might be related to the community shifts from the natural assemblage to large, heavily-silicified diatoms (Tables 2 and S1, discussed below).

The diatom community responded little to Fe addition at both stations, although the communities after on-deck incubation were surely shifted from the Initial. From the microscopic observations, changes in the community composition of phytoplankton at the genus level were few after Fe addition at both stations (Tables 2 and S1). The genus *Chaetoceros* , which was dominated in each bottle, might outcompete under Fe-replete conditions, as observed in other onboard Fe amendment incubations (Timmermans et al., 2001) and *in situ* Fe fertilization experiments (Tsuda et al., 2003). Our study demonstrated that Fe addition stimulated some specific diatom species (e.g., *Pseudo-nitzschia* spp. and *Cylindrotheca closterium* at stations C5 and A5, respectively), which were minor in the initial *Chaetoceros*-dominated communities (Tables 2 and S1). Smaller cell sizes could benefit the efficiency of their nutrient uptake because of their higher cell surface area to volume ratio (Taguchi, 1976; de Baar et al., 1995; Sunda and Huntsman, 1997). The *Chaetoceros* spp., except the larger *Ch. concavicornis* and resting spores, were not abundant in the +DFB bottles but replaced by much larger diatoms such as *Thalassionema nitzschioides*, *Neodenticula seminae, Corethron pennatum,* and *Asteromphalus* spp. (Table S1). The larger cells might be capable of storing surplus Fe in their larger vacuoles (Sicko-Goad et al., 1984; Raven, 1998; Behrenfeld et al., 2021), which can become an important intracellular Fe source (Maranón et al., 2012, 2015) and support their growth even under Fe-deficient conditions (Wells, 1999; Sugie et al., 2011). Also, Maldonado and Price (1999) demonstrated that Fe bound to DFB could be utilized via the reduction of Fe

by large phytoplankton (> 3 μm) such as diatoms. Therefore, the larger diatoms were able to survive in the +DFB bottles.

The abundance of ultraplanktonic cryptophytes was enhanced by Fe addition, whereas *Synechoccocus* little changed. Increases in the abundance of cryptophytes after Fe addition (Fig. 9) were similar to the results from an *in situ* Fe-manipulated experiment in the WSG during summer (Suzuki et al., 2009). Camoying et al. (2022) demonstrated that cryptophytes are vulnerable to Fe limitation due to low affinity to Fe with reduced Cu-mediated Fe reductase (Behnke and LaRoche, 2020); in turn, Fe amendment stimulates the growth of cryptophytes (Camoying et al., 2022) as observed in our study. Sato et al. (2009) reported an increased abundance of *Synechoccocus* after the Fe enrichment during an *in situ* Fe fertilization experiment of SEEDS II in the WSG. In contrast, Kudo et al. (2006) showed a minor increase in *Synechoccocus* by conducting Fe amendment bottle incubation in the WSG. The different responses to Fe enrichment were partly due to physiological or phylotypic differences in *Synechoccocus* before the Fe amendment and higher microzooplankton grazing pressure in Kudo et al. (2006). Our experiments were also conducted in 9 L bottles, and the high abundance of ciliates and choanoflagellates could enhance the grazing pressure on picoplankton. The abundance of both *Synechoccocus* and cryptophytes in the incubation bottles might be somewhat underestimated, although significant increases in cryptophytes were observed in the +Fe bottles (Fig, 9). Some relatively abundant dinoflagellates (*Prorocentrum* spp. and *Gymnodimium* spp.) could also play as grazers (Table S1).

This study first reported the elongation of *Neodenticula seminae* chains with +DFB treatment (Fig. 8). In the WSP, *Neodenticula seminae* was often observed in sediment traps (Katsuki et al., 2003; Katsuki and Takahashi, 2005; Onodera et al., 2005). This pennate diatom species might have a strategy to sink rapidly under Fe-limited conditions by their chain elongation, which could play a significant role in the high biological pump efficiency in the western subarctic Pacific (Honda, 2003).

5. Conclusions

This study demonstrated that the photosynthesis of phytoplankton responded differently to increased Fe availability in respect to the mixed layer depths, which consequently controlled their biomass and community composition in HNLC waters of the WSP. Even though the macro-nutrient and Fe concentrations were similar, vertical mixing significantly affected the photo-acclimation status and, consequently, Fe requirement of

phytoplankton communities: low light acclimation caused Fe limitation in the deep-mixed water. The upward fluxes of DFe and NO_3 were much higher in the deep-mixed water than in the shallow-mixed one. However, as mentioned above, both waters were potentially Fe-limited, inferred from the low F_{DFe}/F_{NO3} ratio. Indeed, the on-deck Fe manipulation confirmed Fe limitation in the deep-mixed water, while the Fe amendment showed little changes in the abundance and photophysiology of phytoplankton in the shallow-mixed water. However, carbon fixation rates little changed in the Fe-limited community, whereas those for the Fe-replete community were enhanced, which indicates different allocative strategies of the energy produced from the improved photosynthetic machinery by the Fe augmentation: chl *a* or carbon fixation. This different response might be related to the size of photosynthetic antennae as an overcoming strategy against the Fe-light co-limitation. Additionally, at the shallow mixed water station, a decrease in the level of cellular chl *a* in Fe-starved phytoplankton may become a superior survival strategy to protect the cells from high irradiance that can cause photo-oxidative damages through photosynthesis (Sugie et al., 2011). Although Fe amendment increased large and/or chain-forming *Chaetocetos* species and cryptophytes, Fe depletion enhanced the abundance of heavily-silicified species (e.g., *N. seminae*) and resting spores observed in the +DFB bottles. This response implies that Fe depletion in the WSP during summer leads to large and heavily-silicified phytoplankton, which enhances the efficiency of the biological pump (Tréguer et al., 2017).

Acknowledgements

We thank the officers and crew of R/V *Professor Multanovskiy*. Thanks also extended to Dr. Y. N. Volkov and the late Mr. Scherbinin, the Far Eastern Regional Hydrometeorological Research Institute, for cooperation under the Japanese-Russian joint research program. We acknowledge Ms. Suzu Nakamura, Ms. Natsuko Araki, and Ms. Aiko Murayama for their shipboard and on-land assistance. This study was partly supported by the JSPS Grant-in-Aid for Scientific Research (JP17H00775, JP18H03352, JP21H05056, JP22H05205, JP21H04921, JP23H03516) funded to JN, KS, and IY, and the Joint Research Program of the Institute of Low Temperature Science, Hokkaido University, and JAXA 2nd Research Announcement on the Earth Observations, Japan Aerospace Exploration Agency (ER2GCF304). KY was partly supported by the Sasakawa Scientific Research Grant from The Japan Science Society (27-752).

Compliance and Ethical Standards

The authors declare that they have no conflicts of interest.

References

Alderkamp AC, Van Dijken GL, Lowry KE, Lewis KM, Joy-Warren HL, Van De Poll W, Laan P, Gerringa L, Delmont TO, Jenkins BD, Arrigo KR (2019) Effects of iron and light availability on phytoplankton photosynthetic properties in the Ross Sea. Mar Eco. Prog Ser 621: 33–50. https://doi.org/10.3354/meps13000

Behrenfeld MJ, Halsey KH, Boss E, Karp-Boss L, Milligan AJ, Peers G (2021) Thoughts on the evolution and ecological niche of diatoms. Ecol Monogr 91: e01457. https://doi.org/10.1002/ecm.1457Behrenfeld MJ, Milligan AJ (2013) Photophysiological expressions of iron stress in phytoplankton. Ann Rev Mar Sci 5: 217–246. https://doi.org/10.1146/annurev-marine-121211-172356

Bouman HA, Platt T, Doblin M, Figueiras FG, Gudmundsson K, Gudfinnsson HG, Huang B, Hickman A, Hiscock M, Jackson T, Lutz VA, Mélin F, Rey F, Pepin P, Segura V, Tilstone GH, Van Dongen-Vogels V, Sathyendranath S (2018) Photosynthesis-irradiance parameters of marine phytoplankton: Synthesis of a global data set. Earth Syst Sci Data 10: 251–266. https://doi.org/10.5194/essd-10-251-2018

Boyd PW, Jickells T, Law CS, Blain S, Boyle EA, Buesseler KO, Coale KH, Cullen JJ, de Baar HJW, Follows M, Harvey M, Lancelot C, Levasseur M, Owens NPJ, Pollard R, Rivkin RB, Sarmiento J, Schoemann V, Smetacek V, Takeda S, Tsuda A, Turner S, Watson AJ (2007) Mesoscale iron enrichment experiments 1993-2005: synthesis and future directions. Science 315: 612–617. https://doi.org/10.1126/science.1131669

Browning T, Achterberg E, Rapp I, Engel A, Bertrand EM, Tagliabue A, Moore CM (2017) Nutrient co-limitation at the boundary of an oceanic gyre. Nature 551: 242–246. https://doi.org/10.1038/nature24063

Camoying MG, Thoms S, Geuer JK, Koch BP, Bischof K, Trimborn S (2022) In contrast to diatoms, cryptophytes are susceptible to iron limitation, but not ocean acidification. Physiol Plant 174: e13614. https://doi.org/10.1111/ppl.13614

de Baar HJW, Boyd PW, Coale KH, Landry MR, Tsuda A, Assmy P, Bakker DCE, Bozec Y, Barber RT,

Brzezinski MA, Buesseler KO, Boyé M, Croot PL, Gervais F, Gorbunov MY, Harrison PJ, Hiscock WT, Laan P, Lancelot C. Law CS, Levasseur M, Marchetti A, Millero FJ, Nishioka J, Nojiri Y, van Oijen T, Riebesell U, Rijkenberg MJA, Saito H, Takeda S, Timmermans KR, Veldhuis MJW, Waite AM, Wong CS (2005) Synthesis of iron fertilization experiments: From the iron age in the age of enlightenment. J Geophys Res C Ocean 110: 1–24. https://doi.org/10.1029/2004JC002601

D'Haene SE, Sobotka R, Bučinská L, Dekker JP, Komenda J (2015) Interaction of the PsbH subuni twith a chlorophyll bound to histidine 114 of CP47 is responsible for the red 77 K fluorescence of Photosystem II. Biochim Biophys Acta 1847: 1327–1334. http://dx.doi.org/10.1016/j.bbabio.2015.07.003

Endo H, Yoshimura T, Kataoka T, Suzuki K (2013) Effects of CO_2 and iron availability on phytoplankton and eubacterial community compositions in the northwest subarctic Pacific. J Exp Mar Bio Ecol 439: 160–175. https://doi.org/10.1016/j.jembe.2012.11.003

Fujiki T, Matsumoto K, Mino Y, Sasaoka K, Wakita M, Kawakami H, Honda MC, Watanabe S, Saino T (2014) Seasonal cycle of phytoplankton community structure and photophysiological state in the western subarctic gyre of the North Pacific. Limnol Oceanogr 59: 887–900. https://doi.org/10.4319/lo.2014.59.3.0887

Geider RJ, LaRoche J (1994) The role of iron in phytoplankton photosynthesis, and the potential for iron-limitation of primary productivity in the sea. Photosynth Res 39: 275–301.

Greene RM, Geider RJ, Kolber Z, Falkowski PG (1992) Iron-induced changes in light harvesting and photochemical energy conversion processes in eukaryotic marine algae. Plant Physiol 100: 565–575. https://doi.org/10.1104/pp.100.2.565

Goto Y, Yasuda I, Nagasawa M (2016) Turbulence estimation using fast-response thermistors attached to a free-fail vertical microstructure profiler. J Atmos Ocean Technol 33: 2065–2078. https://doi.org/10.1175/JTECH-D-15-0220.1

Goto Y, Yasuda I, Nagasawa M (2018) Comparison of turbulence intensity from CTD-attached and free-fall microstructure profilers. J Atmos Ocean Technol 35: 147–162. https://doi.org/10.1175/JTECH-D-17-0069.1

Goto Y, Yasuda I, Nagasawa M, Kouketsu S, Nakano T (2021) Estimation of basin-scale turbulence distribution in the North Pacific Ocean using CTD-attached thermistor measurements. Sci Rep 11: 1–13.

https://doi.org/10.1038/s41598-020-80029-2

Hama T, Miyazaki T, Ogawa Y, Iwakuma T, Takahashi M, Otsuki A, Ichimura S (1983) Measurement of photosynthetic production of a marine phytoplankton population using a stable ^{13}C isotope. Mar Biol 73: 31–36.

Harrison PJ, Boyd PW, Varela DE, Takeda S, Shiomoto A, Odate T (1999) Comparison of factors controlling phytoplankton productivity in the NE and NW subarctic Pacific gyres. Prog Oceanogr 43: 205–234. https://doi.org/10.1016/S0079-6611(99)00015-4

Hattori-Saito A, Nishioka J, Ono T, McKay RML, Suzuki K (2010) Iron deficiency in micro-sized diatoms in the Oyashio region of the Western subarctic Pacific during spring. J Oceanogr 66: 105–115. https://doi.org/10.1007/s10872-010-0009-9

Honda MC (2003) Biological pump in northwestern North Pacific. J Oceanogr 59: 671–684. https://doi.org/10.1023/B:JOCE.0000009596.57705.0c

Hooker SB, Lind RN, Morrow JW, Kudela RM, Housekeeper HF, Suzuki K (2018) Advances in above- and in-water radiometry, Vol. 2: Autonomous atmospheric and Oceanic Observing Systems. TP-2018-219033, Vol. 2, Greenbelt, Maryland: NASA Goddard Space Flight Center, pp. 69.

Hooker SB., Morrow JH, Matsuoka A (2013) Apparent optical properties of the Canadian Beaufort Sea—Part 2: The 1% and 1 cm perspective in deriving and validating AOP data products. Biogeosciences, 10, 4511–4527. https://doi.org/10.5194/bg-10-4511-2013

Hurlbert HH (1984) Pseudoreplication and the design of ecological field experiments. Ecol Monogr 54: 187−211. https://doi.org/10.2307/1942661

Hutchins DA, Franck VM, Brzezinski MA, Bruland KW (1999) Inducing phytoplankton iron limitation in iron-replete coastal waters with a strong chelating ligand. Limnol Oceanogr 44: 1009–1018. https://doi.org/10.4319/lo.1999.44.4.1009

Kaneko H, Itoh S, Kouketsu S, Okunishi T, Hododa S, Suga T (2015) Evolution and modulation of a poleward-propagating anticyclonic eddy along the Japan and Kuril-Kamchatka Trench. J Geophys Res Ocean 120: 4418–4440. https://doi.org/10.1088/1751-8113/44/8/085201

Kaneko H, Yasuda I, Komatsu K, Itoh S (2013) Observations of vertical turbulent nitrate flux across the

Kuroshio. Geophys Res Lett 40: 3123–3127. https://doi.org/10.1002/grl.50613.

Katsuki K, Takahashi K (2005) Diatoms as paleoenvironmental proxies for seasonal productivity, sea-ice and surface circulation in the Bering Sea during the late Quaternary. Deep Res II 52: 2110–2130. https://doi.org/10.1016/j.dsr2.2005.07.001

Katsuki K, Takahashi K, Okada M (2003) Diatom assemblage and productivity changes during the last 340,000 years in the subarctic Pacific. J Oceanogr 59: 695–707. https://doi.org/10.1023/B:JOCE.0000009598.93075.78

Kawakami H, Honda MC, Matsumoto K, Wakita M, Kitamura M, Fujiki T, Watanabe S (2015) POC fluxes estimated from ^{234}Th in late spring-early summer in the western subarctic North Pacific. J Oceanogr 71: 311–324. https://doi.org/10.1007/s10872-015-0290-8

Kawakami H, Yang YL, Honda MC, Kusakabe M (2004) Particulate organic carbon fluxes estimated from ^{234}Th deficiency in winters and springs in the northwestern North Pacific. Geochem J 38: 581–592. https://doi.org/10.2343/geochemj.38.581

Kirk JT (2010) Light and photosynthesis in aquatic ecosystems, 3rd ed., Cambridge: Cambridge University Press.

Kolber ZS, Prášil O, Falkowski PG (1998) Measurements of variable chlorophyll fluorescence using fast repetition rate techniques: Defining methodology and experimental protocols. Biochim Biophys Acta 1367: 88–106. https://doi.org/10.1016/S0005-2728(98)00135-2

Kondo Y, Takeda S, Nishioka J, Sato M, Saito H, Suzuki K, Furuya K (2013) Growth stimulation and inhibition of natural phytoplankton communities by model organic ligands in the western subarctic Pacific. J Oceanogr 69: 97–115. https://doi.org/10.1007/s10872-012-0160-6

Konno S, Ohira R, Harada N, Jordan RW (2007) Six new taxa of subarctic Parmales (Chrysophyceae). J Nannoplankt Res 29: 108–128.

Kudo I, Noiri Y, Nishioka J, Taira Y, Kiyosawa H, Tsuda A (2006) Phytoplankton community response to Fe and temperature gradients in the NE (SERIES) and NW (SEEDS) subarctic Pacific Ocean. Deep-Sea Res II 53: 2201–2213. https/doi.org/10.1016/j.dsr2.2006.05.033

MacIntyre HL, Kana TM, Anning T, Geider RJ (2002) Photoacclimation of photosynthesis irradiance response

curves and photosynthetic pigments in microalgae and cyanobacteria. J Phycol 38: 17–38. https://doi.org/10.1046/j.1529-8817.2002.00094.x

Maldonado MT, Boyd PW, Harrison PJ, Price NM (1999) Co-limitation of phytoplankton growth by light and Fe during winter in the NE subarctic Pacific Ocean. Deep Res Part II 46: 2475–2485. https://doi.org/10.1016/S0967-0645(99)00072-7

Maldonado MT, Price NM (1999) Utilization of Fe bound to strong organic ligands by phytoplankton communities in the subarctic Pacific Ocean. Deep Res II 46: 2447–2473. https://doi.org/10.1016/S0967-0645(99)00071-5

Maranón E, Cermeno P, Latasa M, Tadonléké RD (2012) Temperature, resources, and phytoplankton size structure in the ocean. Limnol Oceanogr 57:1266–1278. https://doi.org/10.4319/lo.2012.57.5.1266

Maranón E, Cermeno P, Latasa M, Tadonléké RD (2015) Resource supply alone explains the variability of marine phytoplankton size structure. Limnol Oceanogr 60:1848–1854. https://doi.org/10.1002/lno.10138

McKay RML, Geider RJ, LaRoche J (1997) Physiological and biochemical response of the photosynthetic apparatus of two marine diatoms to Fe stress. Plant Physiol 114: 615–622. https://doi.org/10.1104/pp.114.2.615

Medvedeva LA, Nikulina TV (2014) Catalogue of Freshwater Algae of the southern part of the Russian Far East. Vladivostok Dalnauka, Vladivostok.

Monterey G, Levitus S (1997) Seasonal variability of mixed layer depth for the World Ocean. NOAA Atlas NESDIS Vol. 14, Washington DC: U. S. Government Printing Office. pp. 102.

Nishioka J, Hirawake T, Nomura D, Yamashita Y, Ono K, Murayama A, Shcherbinin A, Volkov YN, Mitsudera H, Ebuchi N, Wakatsuchi M, Yasuda I (2021) Iron and nutrient dynamics along the East Kamchatka Current, western Bering Sea Basin and Gulf of Anadyr. Prog Oceanogr 198: 102662. https://doi.org/10.1016/j.pocean.2021.102662

Nishioka J, Nakatsuka T, Ono K, Volkov YN, Scherbinin A, Shiraiwa T (2014) Quantitative evaluation of iron transport processes in the Sea of Okhotsk. Prog Oceanogr 126: 180–193. https://doi.org/10.1016/j.pocean.2014.04.011

Nishioka J, Nakatsuka T, Watanabe YW, Yasuda I, Kuma K, Ogawa H, Ebuchi N, Scherbinin A, Volkov YN,

Shiraiwa T, Wakatsuchi M (2013) Intensive mixing along an island chain controls oceanic biogeochemical cycles. Global Biogeochem Cycles 27: 920–929. https://doi.org/10.1002/gbc.20088

Nishioka J, Obata H (2017) Dissolved iron distribution in the western and central subarctic Pacific: HNLC water formation and biogeochemical processes. Limnol Oceanogr 62: 2004–2022. https://doi.org/10.1002/lno.10548

Nishioka J, Obata H, Ogawa H, Ono K, Yamashita Y, Lee K, Takeda S, Yasuda I (2020) Subpolar marginal seas fuel the North Pacific through the intermediate water at the termination of the global ocean circulation. Proc Natl Acad Sci U S A 117: 12665–12673. https://doi.org/10.1073/pnas.2000658117

Nishioka J, Ono T, Saito H, Nakatsuka T, Takeda S, Yoshimura T, Suzuki K, Kuma K, Nakabayashi S, Tsumune D, Mitsudera H, Johnson WK, Tsuda A (2007) Iron supply to the western subarctic Pacific: Importance of iron export from the Sea of Okhotsk. J Geophys Res Ocean 112. https://doi.org/10.1029/2006JC004055

Nishioka J, Takeda S, Wong CS, Johnson WK (2001) Size-fractionated iron concentrations in the northeast Pacific Ocean: Distribution of soluble and small colloidal iron. Mar Chem 74: 157–179. https://doi.org/10.1016/S0304-4203(01)00013-5

Nosaka Y, Isada T, Kudo I, Saito H, Hattori H, Tsuda A, Suzuki K (2014) Light utilization efficiency of phytoplankton in the Western Subarctic Gyre of the North Pacific during summer. J Oceanogr 70: 91–103. https://doi.org/10.1007/s10872-013-0217-1

Nosaka Y, Yamashita Y, Suzuki K (2017) Dynamics and origin of transparent exopolymer particles in the Oyashio region of the western subarctic Pacific during the spring diatom bloom. Front Mar Sci 4: 1–16. https://doi.org/10.3389/fmars.2017.00079

Obata H, Karatani H, Matsui M, Nakayama E (1997) Fundamental studies for chemical speciation of iron in seawater with an improved analytical method. Mar Chem 56: 97–106.

Obata H, Karatani H, Nakayama E (1993) Automated determination of iron in seawater by chelating resin concentration and chemiluminescence detection. Anal Chem 65: 1524–1528. https://doi.org/10.1021/ac00059a007

Ono K, Ohshima KI, Kono T, Itoh M, Katsumata K, Volkov YN, Wakatsuchi M (2007) Water mass exchange

and diapycnal mixing at Bussol' Strait revealed by water mass properties. J Oceanogr 63: 281–291. https://doi.org/10.1007/s10872-007-0028-3

Onodera J, Takahashi K, Honda MC (2005) Pelagic and coastal diatom fluxes and the environmental changes in the northwestern North Pacific during December 1997-May 2000. Deep Res II 52: 2218–2239. https://doi.org/10.1016/j.dsr2.2005.07.005

Osborn TR (1980) Estimates of the local rate of vertical diffusion from dissipation measurements. J Phys Oceanogr 10: 83–89. https://doi.org/10.1175/1520-0485(1980)010<0083:EOTLRO>2.0.CO;2

Osborn TR, Cox CS (1972) Oceanic fine structure. Geophys Fluid Dyn 3: 321–345.

Platt T, Gallegos CL, Harrison WG (1980) Photoinhibition of photosynthesis in natural assemblages of marine phytoplankton. J Mar Res 38: 687–701. https://doi.org/citeulike-article-id:3354339

Raven JA (1995) Scaling the seas. Plant Cell Environ 18:1090–1100. https://doi.org/10.1111/j.1365-3040.1995.tb00621.x

Round FE, Crawford RM, Mann DG (2007) The Diatom: Biology & Morphology of the Genera. Cambridge University Press, Cambridge.

Sakshaug E, Bricaud A, Dandonneau Y, Falkowski PG, Kiefer DA, Legendre L, Morel A, Parslow J, Takahashi M (1997) Parameters of photosynthesis: definitions, theory and interpretation of results. J Plankton Res 19: 1637–1670. https://doi.org/10.1093/plankt/19.11.1637

Sato H, Takeda S, Furuya K (2009) Responses of pico- and nanophytoplankton to artificial iron infusions observed during the second iron enrichment experiment in the western subarctic Pacific (SEEDS II). Deep-Sea Res II 56: 2745−2754. https://doi.org/10.1016/j.dsr2.2009.06.002

Schaeffer BA, Kurtz JC. Hein MK (2012) Phytoplankton community composition in nearshore coastal waters of Louisiana. Mar Pollut Bull 64: 1705-1712. https://doi.org/10.1016/j.marpolbul.2012.03.017

Shaked Y, Twining BS, Tagliabue A, Maldonado MT (2021) Probing the bioavailability of dissolved iron to marine eukaryotic phytoplankton using in situ single cell iron quotas. Glob Biogeochem Cycles 35: e2021GB006979. https://doi.org/10.1029/2021GB006979

Sicko-Goad LM, Schelske CL, Stoermer EF (1984) Estimation of intracellular carbon and silica content of diatoms from natural assemblages using morphometric techniques. Limnol Oceanogr 29: 1170−1178.

https://doi.org/10.4319/lo.1984.29.6.1170

Strzepek RF, Boyd PW, Sunda WG (2019) Photosynthetic adaptation to low iron, light, and temperature in Southern Ocean phytoplankton. Proc Natl Acad Sci U S A 116: 4388–4393. https://doi.org/10.1073/pnas.1810886116

Strzepek RF, Hunter KA, Frew RD, Harrison PJ, Boyd PW (2012) Iron-light interactions differ in Southern Ocean phytoplankton. Limnol Oceanogr 57: 1182–1200. https://doi.org/10.4319/lo.2012.57.4.1182

Suggett DJ, Moore CM, Hickman AE, Geider RJ (2009) Interpretation of fast repetition rate (FRR) fluorescence: signatures of phytoplankton community structure versus physiological state. Mar Ecol Prog Ser 376: 1–19. http://doi.org/10.3354/meps07830

Sugie K, Kuma K, Fujita S, Ushizaka S, Suzuki K, Ikeda T (2011) Importance of intracellular Fe pools on growth of marine diatoms by using unialgal cultures and on the Oyashio region phytoplankton community during spring. J Oceanogr 67: 183–196. https://doi.org/10.1007/s10872-011-0017-4

Sugie K, Nishioka J, Kuma K, Volkov YN, Nakatsuk T (2013) Availability of particulate Fe to phytoplankton in the Sea of Okhotsk. Mar Chem 152: 20–31. https://doi.org/10.1016/j.marchem.2013.03.005

Sunda WG, Huntsman SA (1997) Interrelated influence of iron, light and cell size on marine phytoplankton growth. Nature 390: 389–392. https://doi.org/10.1038/37093

Sunda WG, Huntsman SA (1995) Iron uptake and growth limitation in oceanic and coastal phytoplankton. Mar Chem 50: 189–206.

Suzuki K, Hattori-Saito A, Sekiguchi Y, Nishioka J, Shigemitsu M, Isada T, Liu H, McKay RML (2014) Spatial variability in iron nutritional status of large diatoms in the Sea of Okhotsk with special reference to the Amur River discharge. Biogeosciences 11: 2503–2517. https://doi.org/10.5194/bg-11-2503-2014

Suzuki K, Hinuma A, Saito H, Kiyosawa H, Liu H, Saino T, Tsuda A (2005) Responses of phytoplankton and heterotrophic bacteria in the northwest subarctic Pacific to in situ iron fertilization as estimated by HPLC pigment analysis and flow cytometry. Prog Oceanogr 64: 167–187. https://doi.org/10.1016/j.pocean.2005.02.007

Suzuki K, Minami C, Liu H, Saino T (2002) Temporal and spatial patterns of chemotaxonomic algal pigments in the subarctic Pacific and the Bering Sea during the early summer of 1999. Deep Res II 49: 5685–5704.

https://doi.org/10.1016/S0967-0645(02)00218-7

Suzuki K, Saito H, Isada T, Hattori-Saito A, Kiyosawa H, Nishioka J, McKay RML, Kuwata A, Tsuda A (2009) Community structure and photosynthetic physiology of phytoplankton in the northwest subarctic Pacific during an in situ iron fertilization experiment (SEEDS-II). Deep Res II 56: 2733–2744. https://doi.org/10.1016/j.dsr2.2009.06.001

Taguchi S (1976) Relationship between photosynthesis and cell size of marine diatoms. J Phycol 12: 185–189. https://doi.org/10.1111/j.1529-8817.1976.tb00499.x

Takahashi T, Sutherland SC, Sweeney C, Poisson A, Metzl N, Tilbrook B, Bates N, Wanninkhof R, Feely RA, Sabine C, Olafsson J, Nojiri Y (2002) Global sea–air CO_2 flux based on climatological surface ocean pCO_2, and seasonal biological and temperature effects. Deep Res II 49: 1601–1622. https://doi.org/10.1016/S0967-0645(02)00003-6

Takeda S, Obata H (1995) Response of equatorial Pacific phytoplankton to subnanomolar Fe enrichment. Mar Chem 50: 219–227. https://doi.org/10.1016/0304-4203(95)00037-R

Timmermans KR, Davey MS, van der Wagt B, Snoek J, Geider RJ, Veldhuis MJW, Gerringa LJA, de Baar HJW (2001) Co-limitation by iron and light of *Chaetoceros brevis*, *C. dichaeta* and *C. calcitrans* (Bacillariophyceae). Mar Ecol Prog Ser 217: 287–297. https://doi.org/10.3354/meps217287

Tomas CR (1997) Identifying Marine Phytoplankton. Academic Press, London.

Tréguer P, Bowler C, Moriceau B, Dutkiewicz S, Gehlen M, Aumont O, Bittner L, Dugdale R, Finkel Z, Iudicone D, Jahn O, Guidi L, Lasbleiz M, Leblanc K, Levy M, Pondaven P (2018) Influence of diatom diversity on the ocean biological carbon pump. Nat Geosci 11: 27–37. https://doi.org/10.1038/s41561-017-0028-x

Tsuda A, Takeda S, Saito H, Nishioka J, Nojiri Y, Kudo I, Kiyosawa H, Shiomoto A, Imai K, Ono T, Shimamoto A, Tsumune D, Yoshimura T, Aono T, Hinuma A, Kinugasa M, Suzuki K, Sohrin Y, Noiri Y, Tani H, Deguchi Y, Tsurushima N, Ogawa H, Fukami K, Kuma K, Saino T (2003) A mesoscale iron enrichment in the western subarctic Pacific induces a large centric diatom bloom. Science 300: 958–961. https://doi.org/10.1126/science.1082000

Twining BS, Baines SB (2013) The trace metal composition of marine phytoplankton. Ann Rev Mar Sci 5: 191–

215. https://doi.org/10.1146/annurev-marine-121211-172322

Wahl RJ, Teague WJ (1983) Estimation of Brunt-Väisälä frequency from temperature profiles. J Phys Oceanogr 13: 2236–2240. https://doi.org/10.1175/1520-0485(1983)013<2236:EOBVFF>2.0.CO;2

Wells ML (1999) Manipulating iron availability in nearshore waters. Limnol Oceanogr 44: 1002–1008.

Yagi M, Yasuda I (2012) Deep intense vertical mixing in the Bussol' Strait. Geophys Res Lett 39: 1–5. https://doi.org/10.1029/2011GL050349

Yasuda I (2000) Cold-core anticyclonic eddies south of the Bussol' Strait in the Northwestern subarctic Pacific. J Phys Oceanogr 30: 1137–1157.

Yasuda I, Fujio S, Yanagimoto D, Lee KJ, Sasaki Y, Zhai S, Tanaka M, Itoh S, Tanaka T, Hasegawa D, Goto Y, Sasano D (2021) Estimate of turbulent energy dissipation rate using free-fall and CTD-attached fast-response thermistors in weak ocean turbulence. J Oceanogr 77: 17–28. https://doi.org/10.1007/s10872-020-00574-2

Yoshida K, Endo H, Lawrenz E, Isada T, Hooker SB, Prášil O, Suzuki K (2018) Community composition and photophysiology of phytoplankton assemblages in coastal Oyashio waters of the western North Pacific during early spring. Estuar Coast Sci 218: 218: 80−94. https://doi.org/10.1016/j.ecss.2018.06.018

Yoshida K, Nakamura S, Nishioka J, Hooker SB, Suzuki K (2020) Community composition and photosynthetic physiology of phytoplankton in the western subarctic Pacific near the Kuril Islands with special reference to iron availability. J Geophys Res Biogeosciences 125: e2019JG005525. https://doi.org/10.1029/2019JG005525

Yoshimura T, Nishioka J, Nakatsuka T (2010) Iron nutritional status of the phytoplankton assemblage in the Okhotsk Sea during summer. Deep Res I 57: 1454–1464. https://doi.org/10.1016/j.dsr.2010.08.003

Figures

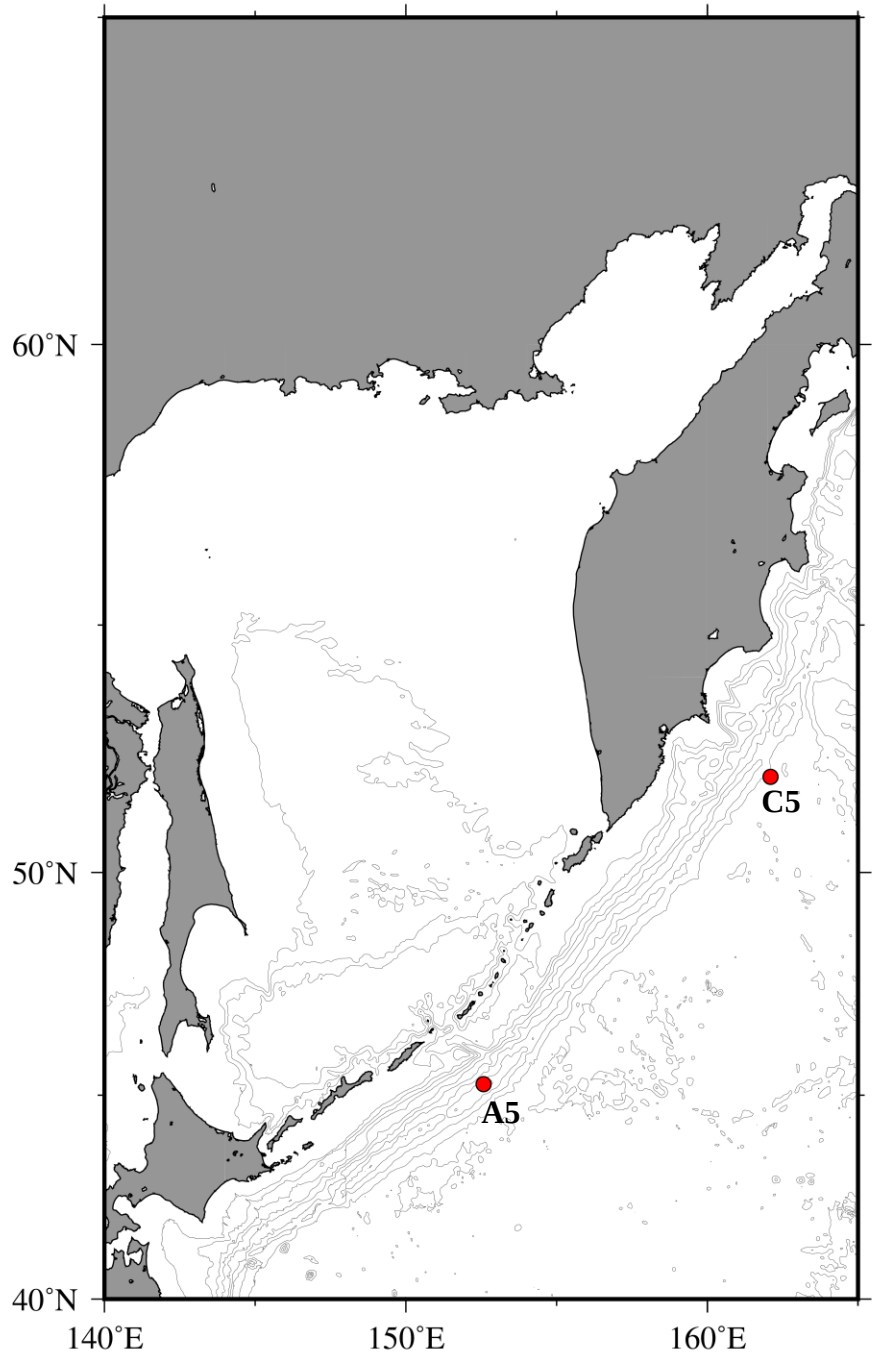

Figure 1. Surface water sampling sites (red circles) for on-deck Fe manipulation incubation experiments in the western subarctic Pacific

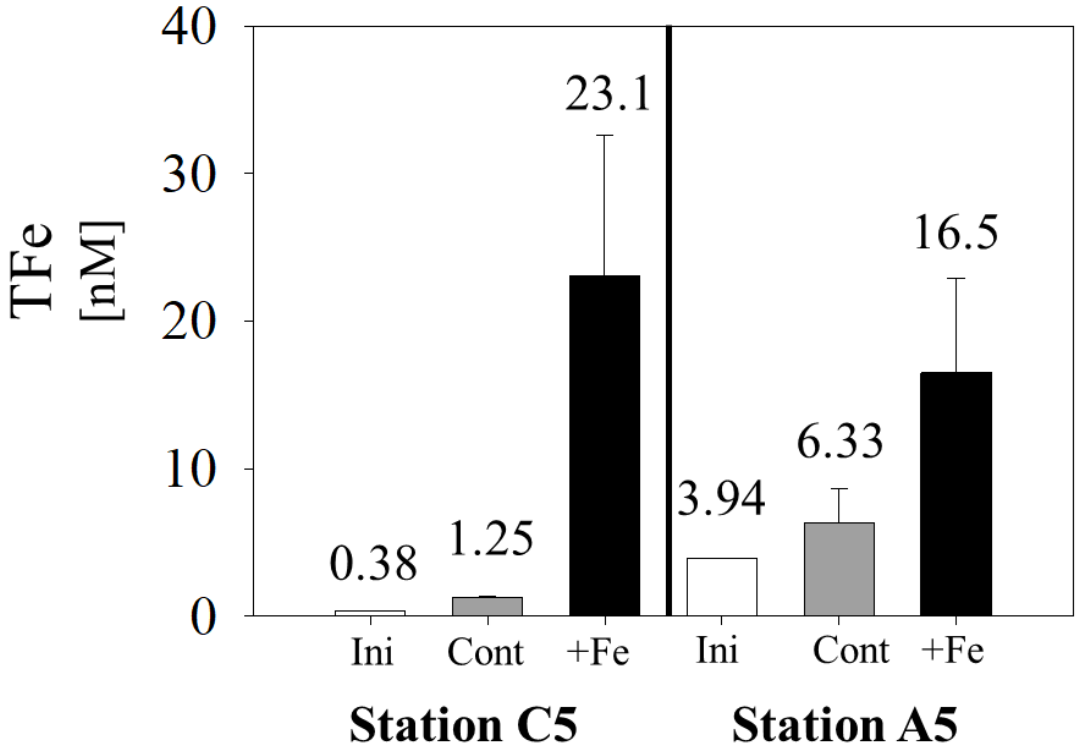

Figure 2. Total dissolvable Fe concentrations throughout the Fe manipulation experiment at stations C5 and A5

Ini (open): Initial treatment, Cont (shaded): Control treatment (closed); +Fe: +Fe treatment (dotted)

The concentrations of TFe in the +DFB treatments were not determined at both stations.

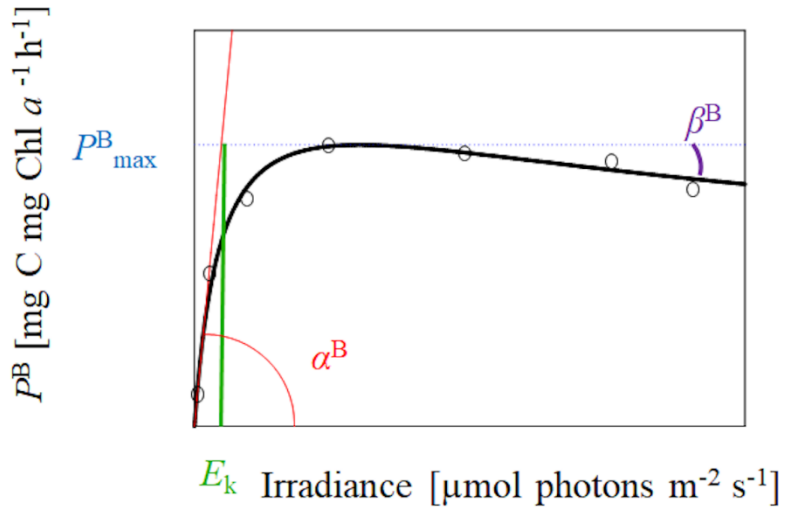

Figure 3. A model photosynthesis–irradiance (*P-E*) curve fitted with Platt et al. (1980).

α^B: Light utilization index [(mg C mg chl a^{-1} hr^{-1}) (µmol photons m^{-2} s^{-1})$^{-1}$]; PBmax: [mg C mg chl a^{-1} hr^{-1}]; E_k [µmol photons m^{-2} s^{-1}]; β^B: Light inhibition index [(mg C mg chl a^{-1} hr^{-1}) (µmol photons m^{-2} s^{-1})$^{-1}$

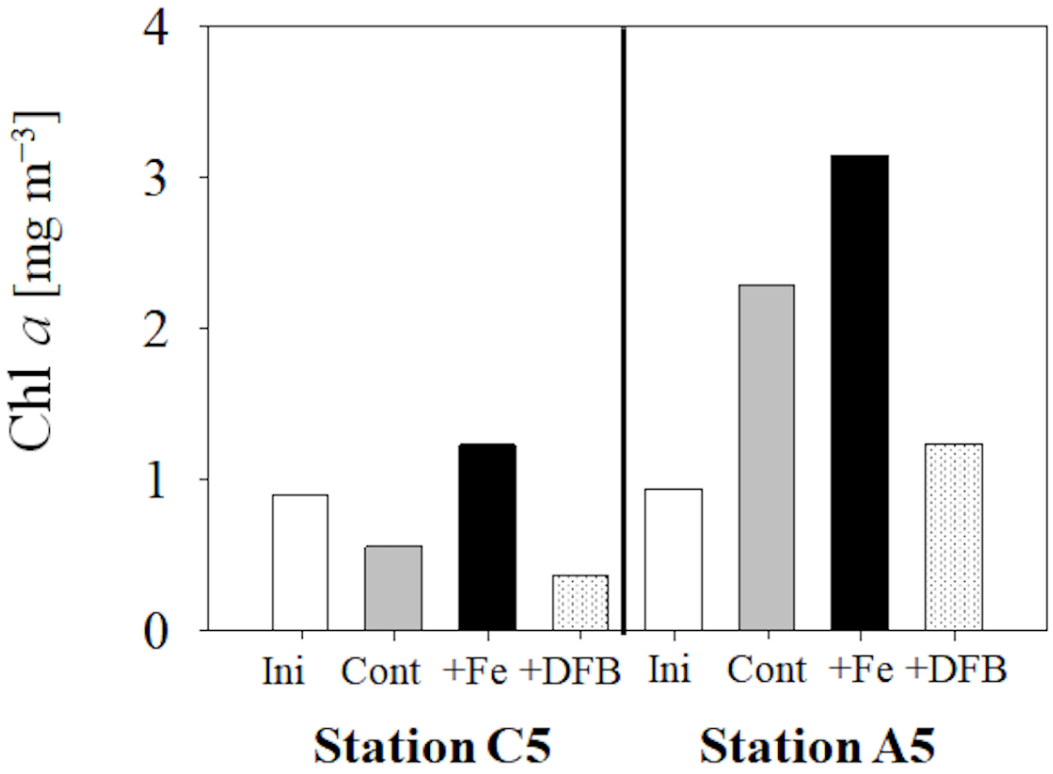

Figure 4. Variations in chl *a* concentration during the on-deck Fe manipulation incubation experiments.

Chl *a*: the sum of chl *a*, chl *a*-epimer, chl *a*-alomer, and chlorophyllide *a*

Ini (open): Initial treatment, Cont (shaded): Control treatment; +Fe (closed): +Fe treatment; +DFB (dotted): +DFB treatment.

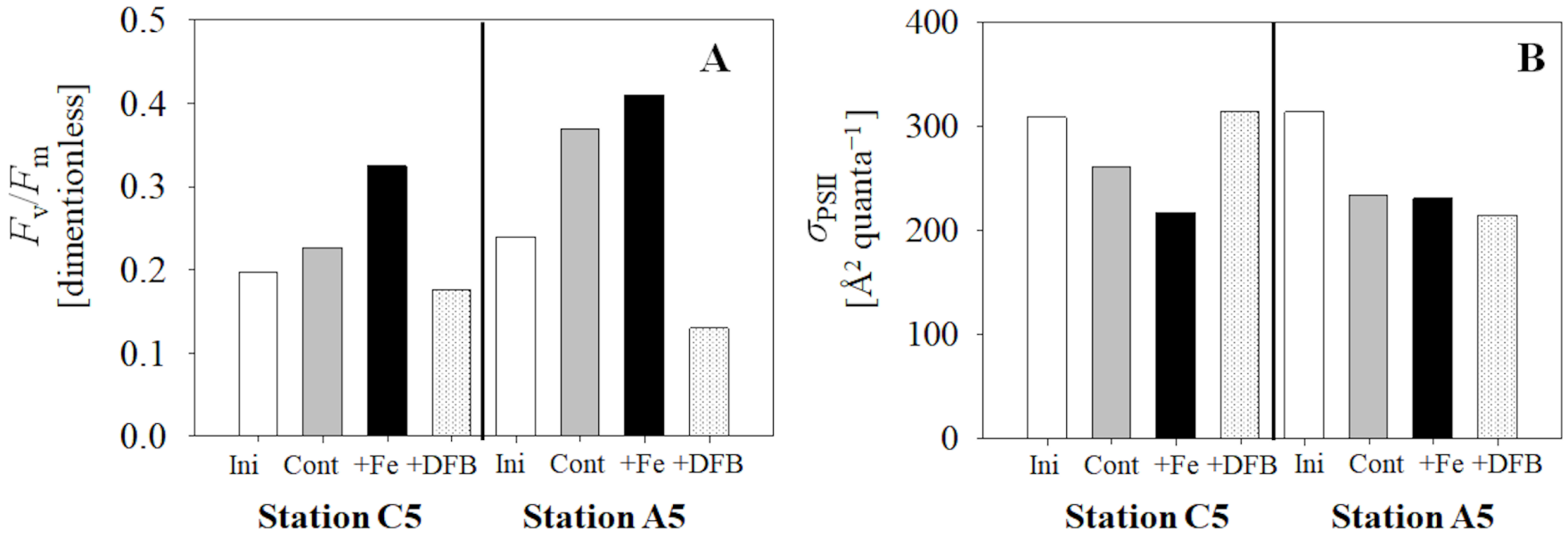

Figure 5. Variations in (A) F_v/F_m and (B) σ_{PSII} [Å^2 quanta^{-1}] during the on-deck Fe manipulation incubation experiments.

F_v/F_m: Maximum quantum yield of PSII photochemistry measured with FIRe fluorometry

σ_{PSII}: Functional absorption cross section of PSII

Ini (open): Initial treatment, Cont (shaded): Control treatment; +Fe (closed): +Fe treatment; +DFB (dotted): +DFB treatment

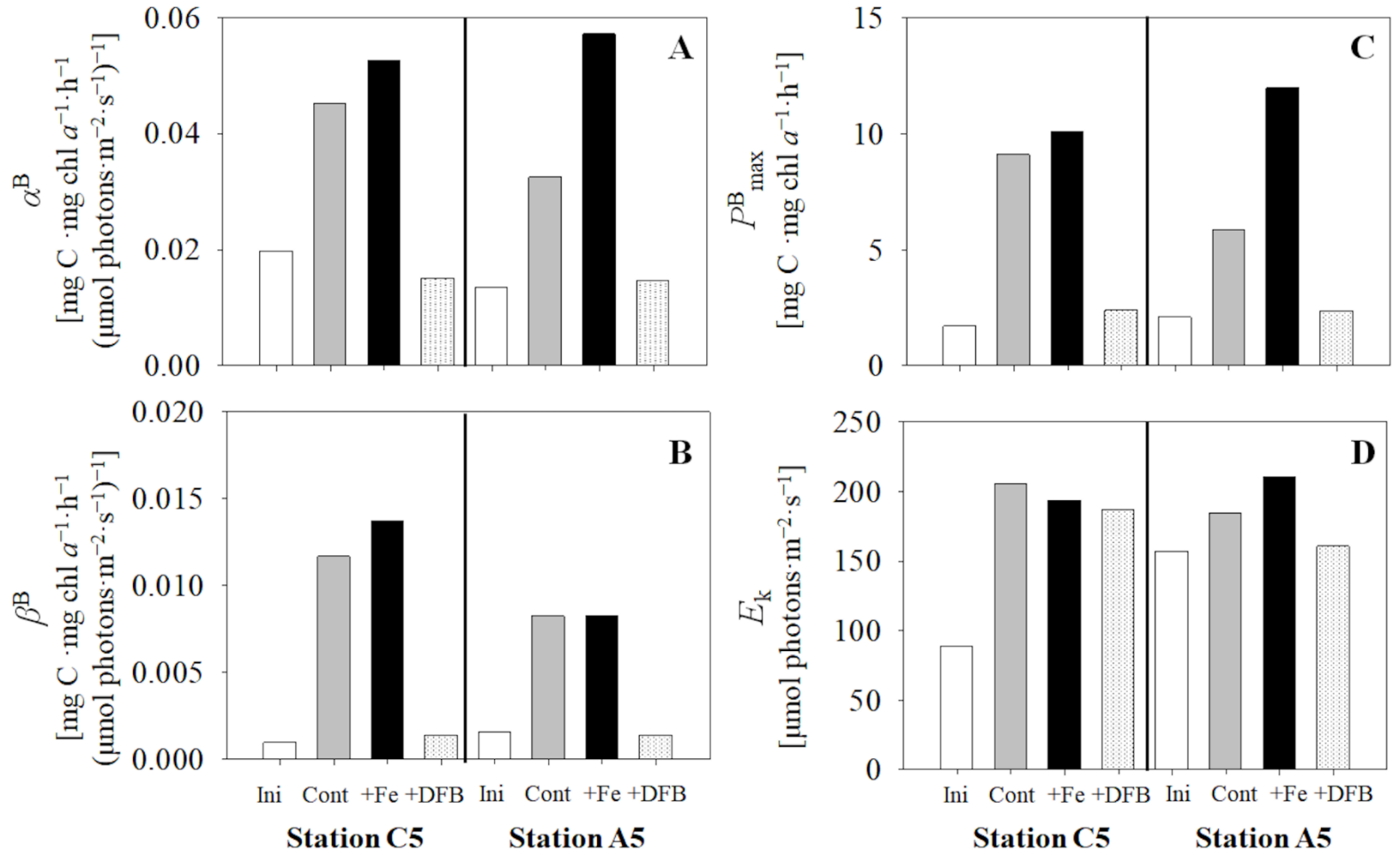

Figure 6. Variations in photophysiological parameters obtained from carbon-based photosynthesis−irradiance relationships; (A) α^B: light utilization index, (B) β^B: photoinhibition index, (C) P^B_{max}: maximum photosynthetic rate, and (D) E_k: Light saturation index

Ini (open): Initial treatment, Cont (shaded): Control treatment; +Fe (closed): +Fe treatment; +DFB (dotted): +DFB treatment

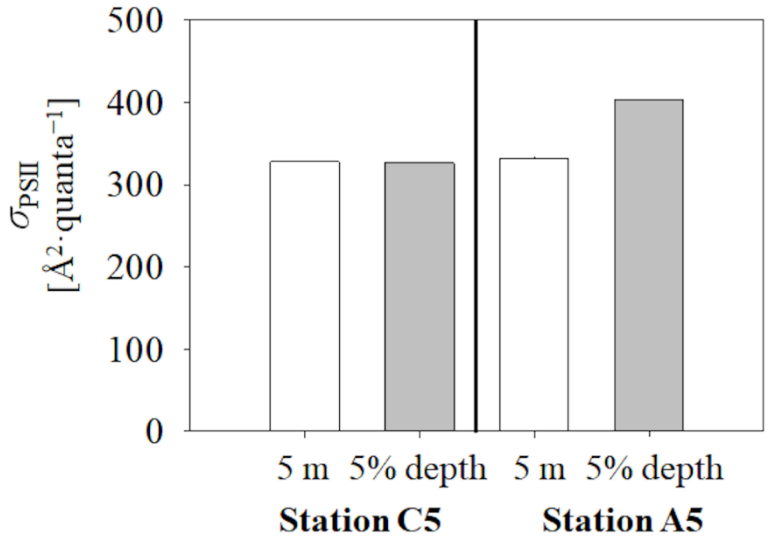

Figure 7. Functional absorption cross-section of PSII (σ_{PSII}) for phytoplankton at the surface (5 m, open) and 5% light depth (5%, shaded) at stations C5 and A5.

The 5% light depth was calculated from the diffusive attenuation coefficient of PAR ($K_{d\ (PAR)}$) (Yoshida et al., 2020).

Differences in σ_{PSII} between 5 m and 5% light depth ($\Delta\sigma_{PSII}$) were smaller ($\Delta\sigma_{PSII} = 2$) at station C5 and larger ($\Delta\sigma_{PSII} = 71$) at station A5, respectively. n =3

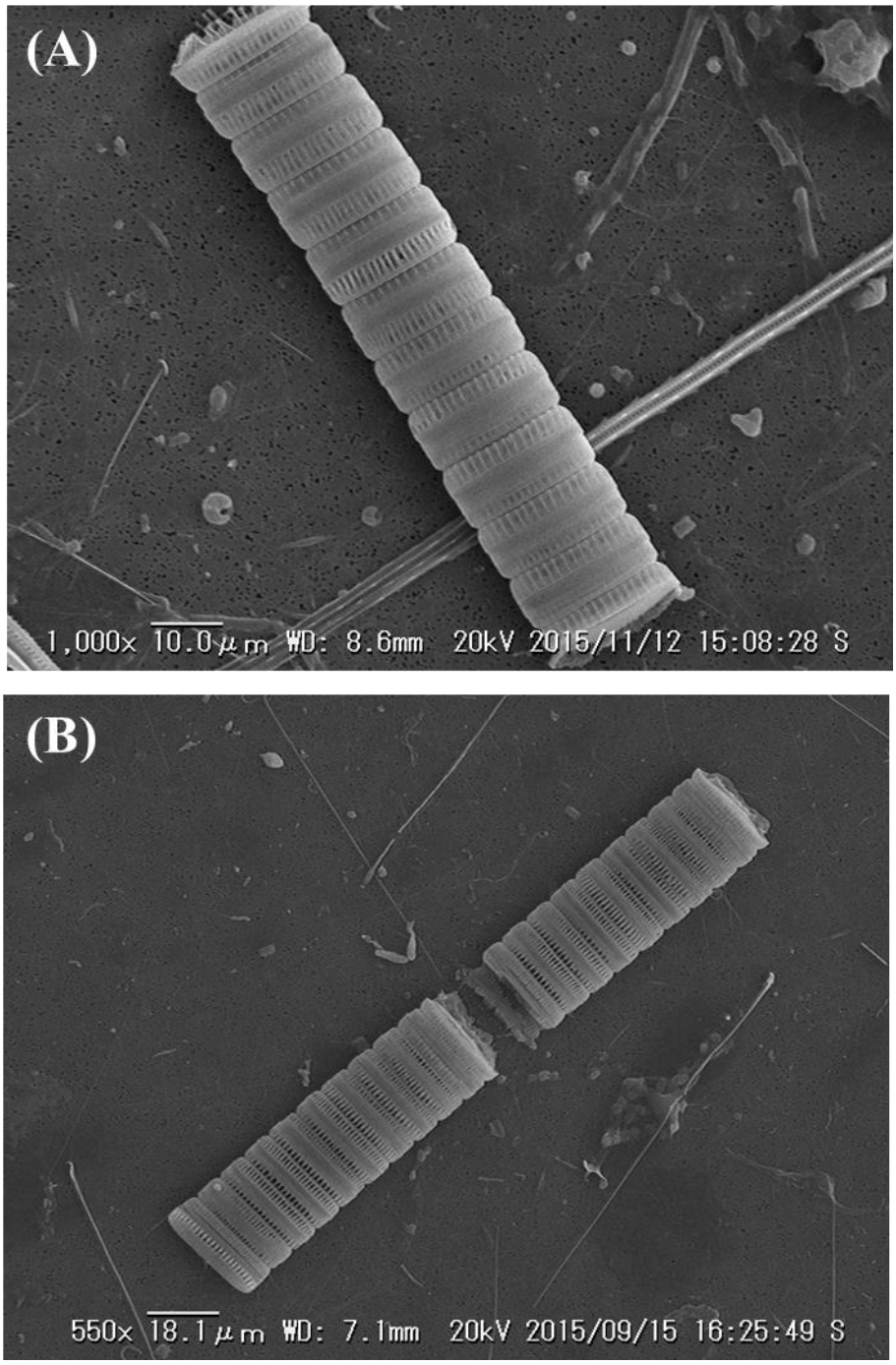

Figure 8. Scanning electron micrographs of the pennate diatom *Neodenticula seminae* with elongated chains from the +DFB bottles (A) at stations C5 and (B) A5.

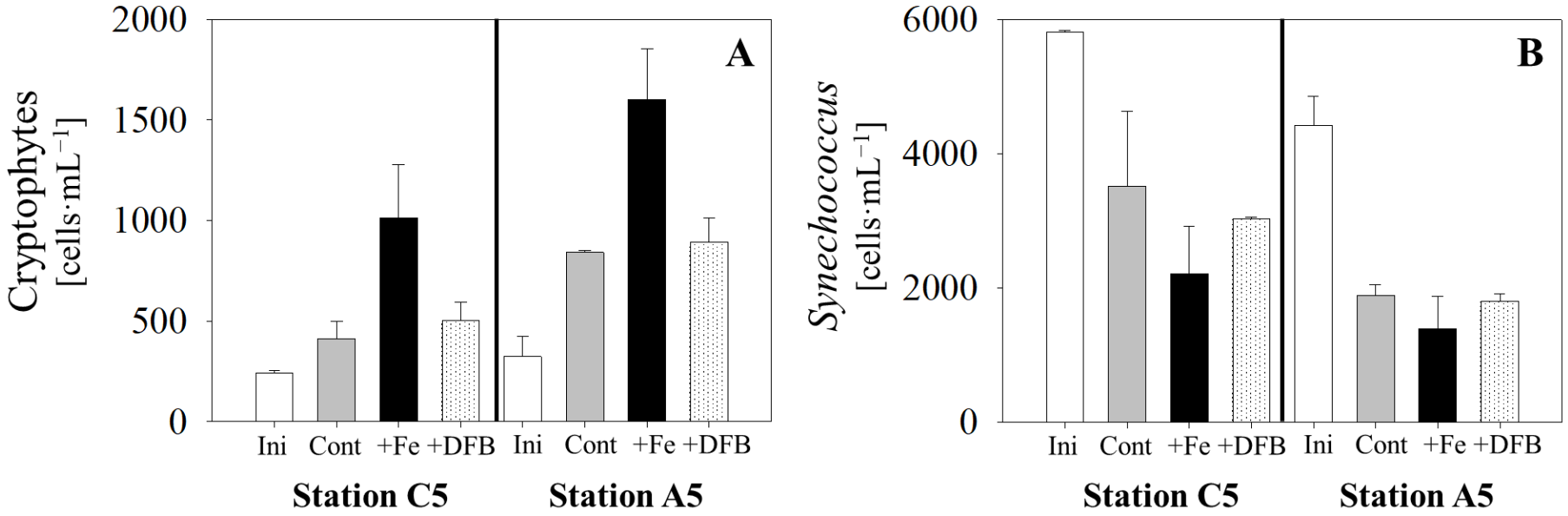

Figure 9. Cell abundance of ultraplankton (<10 μm) enumerated using a flow cytometer. (A) cryptophytes and (B) *Synechococcus*. Ini (open): Initial treatment, Cont (shaded): Control treatment (closed); +Fe: +Fe treatment (dotted)

Tables

Table 1. Environmental parameters during the incubation experiments. (A) Physical and chemical properties of surface waters at Stations C5 and A5. (B) optical properties during the Fe-manipulation incubation experiments.

(A)

		Station C5	Station A5
SST	[°C]	6.05	6.80
SSS	-	32.77	32.81
NO_3	[μM]	9.93	16.64
NO_2	[μM]	0.16	0.27
NH_4	[μM]	0.39	0.3
PO_4	[μM]	1.09	1.53
SiO_4	[μM]	12.91	14.88
DFe	[nM]	0.05	0.06
MLD	[m]	28.5	12.8
Z_{eu}	[m]	40.3	36.2
N^2	[s^{-1}]	9.82×10^{-2}	9.82×10^{-2}
$K_{T\ (10\text{-}50\ m)}$	[$m^2\ s^{-1}$]	1.88×10^{-4}	0.267×10^{-4}
$\partial NO_3/\partial z_{\ (10\text{-}50\ m)}$	[mmol m^{-4}]	173	129
F_{NO3}	[mmol $m^{-2}\ day^{-1}$]	2.82×10^3	297
$\partial DFe/\partial z_{\ (10\text{-}50\ m)}$	[μmol m^{-4}]	2.02	1.35
F_{DFe}	[μmol $m^{-2}\ day^{-1}$]	32.7	3.11
F_{DFe}/F_{NO3}	[nM μM^{-1}]	0.0116	0.0105

SST: sea surface temperature; SSS: sea surface salinity; NO_3: nitrate concentration; NO_2: nitrite concentration; NH_4: ammonium concentration; PO_4; phosphate concentration; SiO_4: silicate concentration; DFe: dissolved iron concentration; MLD: mixed layer depth; Z_{eu}: euphotic zone depth; N^2: 3-m averaged Brunt–Väisälä frequency across the MLD; F_{NO3}, F_{DFe}: upward fluxes of nitrate and DFe, respectively; F_{DFe}/F_{NO3}: ratio of upward fluxes of DFe to NO_3 The surface data and vertical profiles were

adapted from Nishioka et al. (2020, 2021) and Yoshida et al. (2020).

(B)

Station	Treatment	E_0(PAR)max [μmol photons m^{-2} s^{-1}]	E_0(PAR)Ave [μmol photons m^{-2} s^{-1}]
C5	Initial	1111*	–
	Control	1256 ± 358	331 ± 234
	+Fe	1219 ± 341	251 ± 77
	+DFB	1281 ± 309	279 ± 89
A5	Initial	632*	–
	Control	1246 ± 558	341 ± 238
	+Fe	1246 ± 558	304 ± 257
	+DFB	1334 ± 453	313 ± 224

E_0(PAR)ave: daily average incident PAR at the surface during each treatment of the Fe-manipulation incubation experiments; an average value with standard deviation throughout the incubations of each treatment.

Table 2. Contributions of armored protistan plankton to the total plankton in each bottle enumerated with a scanning electron microscope

Treatment		C5_Ini	C5_Cont	C5_+Fe	C5_+DFB	A5_Ini	A5_Cont	A5_+Fe	A5_+DFB
Unidentified		0.7%	1.8%	3.0%	11.3%	9.5%	4.5%	17.7%	20.2%
Coccollithophores		3.2%	0.6%	0.2%					
Parmales		44.4%	5.2%	5.6%	0.1%	0.4%	2.1%	0.0%	0.3%
Silicoflagellate		0.6%	0.3%	0.3%	0.6%	0.2%	0.0%	0.1%	0.3%
Dinoflagellates			0.1%		2.8%	2.4%	0.2%	0.7%	3.2%
Flagellates			0.5%	0.6%	9.0%	0.5%	0.1%		1.1%
Diatoms		**51.0%**	**91.4%**	**89.6%**	**76.2%**	**87.0%**	**93.0%**	**81.5%**	**75.0%**
Centric diatoms	Size (μm)								
Chaetoceros		++++	++++	++++	++	++++	++++	++++	++
C .atlanticus		*	*			**	*	*	**
C. concavicornis	$29.3 \pm 8.3_a^Y$	*	*	*	**	*	*	*	**
C. convolutus	$31.1 \pm 4.8_a^Y$					*	*	*	**
C. deblis	$11.1 \pm 1.7_a^Y$	***	**	**		**	**	*	*
C. diadema	$23.7 \pm 3.2_a^Y$	***	***	**		***	***	**	*
C. furcellatus	$10.3 \pm 1.8_a^Y$	**	**	***		**	**	**	*
Chaetoceros resting spores	–		*	*	***	*		*	*
Other *Chaetoceros*	–	*	**	**	*****	**	***	****	****
Thalassiosira		+	+	+	++	++	+	+	+
T. anguste-lineata	$14–78_v^T$	**				*			
T. bulbosa	$2–16_v^T$	**	**	**	***	*	**	**	
T. nordenskioeldii	$15.0–2.8_v$	**	**	**	**		*		**
T. oceanica	$\sim 3_v$	****	****	****	*	*****	*****	*****	**
Thalassiosira spp.	–	**	**	*	*****	**	*	*	****
Other centric diatoms	–	+	++	++	+++	++	+	+	++
Pennate diatoms									
Cylindrotheca closterium	$\sim 1.7_a^{bY}$		+	+	+	+	+	++	++
Fragilariopsis spp.	$12.5 \pm 7.8_a^Y$	++	++	++	+++	++	++	+	+
Neodenticula seminae	$21.4 \pm 3.7_a^Y$	+	+	+	++	+	+	+	++
Pseudo-nitzschia spp.	$10.3 \pm 1.8_a^Y$	+	+	++	+	+	++	++	++
Other pennate diatoms	–	+	+	+	++	+	+	+	++

Ini: Initial treatment; Cont: Control treatment; +Fe: +Fe treatment; +DFB: +DFB treatment

The contributions of each species were cell-number-based. The microscopic data of the initial bottles were modified from Table 3 of Yoshida et al. (2020).

Contributions of diatoms were indicated with the number of plus (+) symbols: +: >0–5%, ++: >5–25%, +++: >25–50%, ++++: >50%. The contributions of each *Chaetoceros* and *Thalassiosira* species were indicated with the number of asterisks (*) with the same criteria as those of diatoms described above. The contributions of diatoms were independently calculated within diatoms (i.e., excluding other planktonic species; coccolithophores, Parmales, silicoflagellates, dinoflagellates, and flagellates). $_{a}$ apical length; $_{v}$ valve diameter; $_{Y}$ and ^{T} cell size referenced from Yoshida et al. (2020) and Tomas (1997), respectively. [b] The approximate apical length of the diatom *Cylindrotheca closterium* that it was difficult to precisely measure due to their weak silicification and twisted body on the filter for SEM. For more details, see Table S1.